Research Article

Saima Noor and Azzh Saad Alshehry*

Mononuclear nanofluids undergoing convective heating across a stretching sheet and undergoing MHD flow in three dimensions: Potential industrial applications

https://doi.org/10.1515/phys-2023-0170
received October 26, 2023; accepted December 16, 2023

Abstract: The main goal of this study is to analyze the nanofluid boundary layer as it flows over a bidirectional, exponentially extending sheet in both convective and magnetic field environments. The mathematical model considers the results of Brownian motion and particle movement caused by a temperature gradient. Using appropriate similarity transformations, governing partial differential equations are converted into ordinary differential systems, and the design of equations is then solved using the Haar wavelet collocation approach. The findings identify unique trends in the distribution of temperature and show relationships with particular sets of parametric values. These results emphasize how important it is to note temperature fluctuations associated with specific parametric settings. The findings are validated by contrasting the results with similar cases from earlier studies in the literature. The findings indicate that temperature distribution is reduced by increasing the Prandtl number. Additionally, the local Biot number has qualitatively similar effects on temperature and concentration profiles. For higher local Biot numbers, the profiles of concentration and temperature are better.

Keywords: Haar wavelet collocation approach, magnetohydrodynamics flow, convective condition

Nomenclature

c_f	specific heat at constant pressure (J/kg K)
F	non-dimensional stream function
x_1	velocity in x-axis (m/s)
x_2	velocity in y-axis (m/s)
x_3	velocity in z-axis (m/s)
T	fluid temprature (°C)
T_{x_1}	temperature at the stretching surface
T_∞	ambient fluid temperature
ux_1	extensional velocity in x-axis
v_{x_2}	extensional velocity in y-axis
B_0	magnetic field strength
i	time index during navigation
L	scale
t	time
Pr	Prandtl number
V	velocity vector
Re_x	local Reynolds number
C_{fx1}	skin friction coefficient along x-direction
C_{fx2}	skin friction coefficient along y-direction
Nu_x	local Nusselt number
q_{x3}	surface heat flux

Greek symbols

κ	thermal conductivity (W/mK)
μ	thermal viscosity (Ns/m)
ρ	fluid density (kg/m^3)
τ_{x1}	shear force parallel x-axis at the wall
τ_{x2}	shear force parallel y-axis at the wall
$\nu = \mu/\rho$	kinematic viscosity of the fluid
ζ	dimensionless parameter

*** Corresponding author: Azzh Saad Alshehry,** Department of Mathematical Sciences, Faculty of Sciences, Princess Nourah Bint Abdulrahman University, P.O. Box 84428, Riyadh 11671, Saudi Arabia, e-mail: asalshihry@pnu.edu.sa
Saima Noor: Department of Basic Sciences, Preparatory Year, King Faisal University, Al Ahsa 31982, Saudi Arabia, e-mail: snoor@kfu.edu.sa

1 Introduction

Multiple technical methods rely heavily on the stretch surface's ability to facilitate flow and heat transmission. Many scientists have invested time and energy in studying how stretchy thermal covers affect the boundary-layer flow. The authors of the current publication have a particular interest in this domain of study [1,2]. These nanoparticles in suspension can alter the thermal and transport characteristics of the fluid. Recent articles [3,4] examine the challenges of heat transport in nanofluids in light of these applications. Nanoparticles have been the subject of recent research [5,6] in several domains, such as health, materials science, and environmental engineering. Nanoparticles are currently being extensively investigated for their potential in targeted medicine delivery, enhancing material characteristics, and tackling environmental issues such as pollution elimination. Due to their distinctive characteristics, they possess great adaptability and can completely transform technology and provide inventive solutions across several scientific fields. Researchers have found that nanofluids can potentially enhance solar collectors' capacity to absorb solar energy [7–9]. Jena *et al.* [10] proposed a novel mathematical framework that was carefully developed and examined to represent the temporary movement of nanofluid over a vertical surface accurately, which allows the flow to pass through. This study examines the influence of a tilted magnetic field on the movement characteristics of the flow. Numerical solutions for the solar-relevant nonlinear radiation heat transfer problem in nanofluids were derived by Mushtaq *et al.* [11]. In experiments [12], a deformable surface in a boundary layer that was stretched and had temperature fluctuations along the wall was investigated. The goal of this study was to determine how these variables affected the temperature distribution and near-surface dynamics. The PST and PHF are the required minimum and maximum temperatures and heat flows, respectively. It has been noted that for the Sisko fluid material parameter wave movement, the effect is most pronounced at low Prandtl numbers.

Uddin *et al.* [13] examined the effect of thermal variability on the mass transfer of nanofluid under a Newtonian heating condition *via* a stretchy surface implanted into a porous medium. They found that the Newtonian heating parameter significantly affects the temperature. Shen *et al.* [14] studied the vertically stretchable nonlinear surface subject to a constant heat flux. The researchers used a mixed convective boundary fluid to examine the magnetohydrodynamic (MHD) stagnation point flow. Upreti *et al.* [15] investigated the heat transfer characteristics of stagnation point flow, including Casson nanofluid across a stretching sheet. They consider the influence of an induced magnetic field and utilize the Cattaneo–Christov model. This work enhances our comprehension of thermal events in intricate fluid systems.

There are several uses for the heat and mass transfer of MHD thermophoretic flow in different situations, including air purification, aerosol particle monitoring, nuclear reactor safety, and microelectronics production. Particles of micron or less in size suspended in a non-isothermal gas undergo a process known as thermophoresis. They move in the direction of a diminishing thermal gradient. Hsiao [16] studied the problem of boundary-layer flow under mixed convection across a stretching sheet. These are connected to the ongoing study of nanofluid flow. Naramgari and Sulochana [17] have researched a similar boundary-layer problem. They claimed that increasing the magnetic field parameter causes the friction factor to rise and the velocity profiles to slow down. Pandey *et al.* [18] analyzed the MHD properties of a hybrid nanofluid that contains both molybdenum disulfide (MoS_2) and graphene oxide nanoparticles. It specifically investigates the effects of various slip mechanisms, natural convection, and a chemical reaction of "m" order. Hayat *et al.* [19] investigated the behavior of melt polymer in response to a non-uniformly expanding surface of different thicknesses. This study illuminated the complex dynamics between the material and the changing surface structure by examining the interactions between the polymer and the nonlinear stretching sheet. Ghosh and Mukhopadhyay [20] examined how MHD, viscous dissipation, and chemical reactions affected heat transmission and flow of nanofluids embedded in porous media. Upreti and Pandey [21] have used quadratic convection and the Cattaneo–Christov heat flux model to do a statistical analysis of tangent hyperbolic fluid flow across a porous stretching sheet. This study advances our knowledge of the properties of heat transmission in the context of fluid dynamics across porous surfaces and sheds light on the intricate interactions between these variables. Some recent investigations [22–24] have additionally integrated sophisticated nanomaterials, such as magnetic nanoparticles, to control the characteristics of fluids. Applications span from the study of fluid dynamics in biomedicine to the development of sustainable energy systems, demonstrating the wide range of prospective research areas in modern MHD. The effects of chemical processes on heat and mass transfer rates, as well as fluctuations in the thermal boundary layer, are shown by the results of previous studies [25–29].

The impact of a boundary condition when the surface is convective has not been considered in any of these studies. In addition, the radiant heat is typically a fixed value of some other factors in most boundary-layer flow investigations. It is imperative to consider the convective heat

exchange that occurs between the surrounding fluid and the surface in many real-world applications requiring surface cooling or heating. This is also very important when working with thermal materials. Rashidi *et al.* [30] solved a vertically moving flat plate in the traditional problem of radiant heat transfer, taking into account a convective limiting condition (Figure 1).

In this research, we consider a convective surface boundary condition and a transverse magnetic field to investigate the problem of a steady flow of nanofluids over a bidirectional exponentially extending sheet. The mathematical framework offered integrates the results arising from Brownian motion and particle displacement caused by a temperature gradient. These results clarify the appearance of interesting spatial patterns similar to Sparrow–Gregg-type Hills in the temperature distribution. The presence of these characteristics corresponds to specific combinations of parametric values. The validation of these discoveries is accomplished by conducting a comparative analysis with similar scenarios reported in previous literature, confirming the strength and significance of the identified phenomena. The Haar wavelet collocation method (HWCM) [31–33] has been used to compute the nonlinear governing systems. The fluid flow characteristics are examined due to the effects of several intriguing variables. A schematic flowchart of the proposed approach is given in Figure 2.

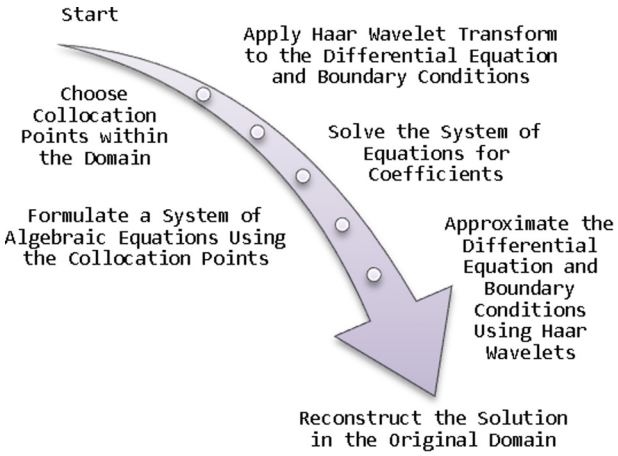

Figure 2: Flowchart illustrating the "HWCM approach."

2 Mathematical formulation

In both the vertical and horizontal planes, investigate the condition of an exponentially stretched sheet and the MHD nanofluid's continuous, incompressible boundary layer flow. The sheet's location is defined as ($x_3 = 0$), and the flow of fluid is limited to the area, where ($x_3 \geq 0$). Assume the velocities of the sheet $u_1(x_1, x_2) = U_0 e^{\left(\frac{x_1+x_2}{L}\right)}$ in the x-direction and $u_2(x_1, x_2) = V_0 e^{\left(\frac{x_1+x_2}{L}\right)}$, the y-direction. When a magnetic field (B_0) is introduced perpendicular to the flow of the fluid, the fluid becomes electrically conductive. It is hypothesized that the induced magnetic field can be regarded as insignificant in comparison with the applied magnetic field because most fluids used in industrial applications have low magnetic Reynolds numbers. As a result, the Hall effect is ignored. $T_{x_3} = T_\infty + u_1 e^{A\left(\frac{x_1+x_2}{2L}\right)}$, which is the temperature at which the sheet is kept, and $C_{x_3} = C_\infty + C_0 e^{A\left(\frac{x_1+x_2}{2L}\right)}$, which is the volume ratio of nanoparticles. T_∞ and C_∞ are the corresponding values at room temperature. The equations regulating the system with boundary conditions are as follows [34–36]:

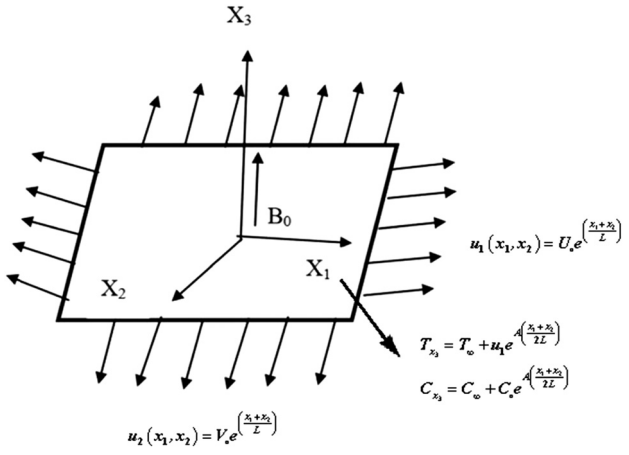

Figure 1: Representation of the spatial configuration and establishment of the coordinate system.

$$\frac{\partial u_1}{\partial x_1} + \frac{\partial u_2}{\partial x_2} + \frac{\partial u_3}{\partial x_3} = 0, \tag{1}$$

$$u_1\frac{\partial u_1}{\partial x_1} + u_2\frac{\partial u_1}{\partial x_3} + u_3\frac{\partial u_1}{\partial x_3} = \nu\frac{\partial^2 u_1}{\partial x_3^2} - \frac{\sigma B_0^2}{\rho}u_1, \tag{2}$$

$$u_1\frac{\partial u_2}{\partial x_1} + u_2\frac{\partial u_2}{\partial x_3} + u_3\frac{\partial u_2}{\partial x_3} = \nu\frac{\partial^2 u_2}{\partial x_3^2} - \frac{\sigma B_0^2}{\rho}u_2, \tag{3}$$

$$\begin{aligned} &u_1\frac{\partial T}{\partial x_1} + u_2\frac{\partial T}{\partial x_3} + u_3\frac{\partial T}{\partial x_3} \\ &= \alpha\frac{\partial^2 T}{\partial x_3^2} + \tau\left[d_b\left(\frac{\partial C}{\partial x_3}\frac{\partial T}{\partial x_3}\right) + \frac{d_t}{d_\infty}\left(\frac{\partial T}{\partial x_3}\right)^2\right], \end{aligned} \tag{4}$$

$$u_1\frac{\partial C}{\partial x_1} + u_2\frac{\partial C}{\partial x_3} + u_3\frac{\partial C}{\partial x_3} = d_b\left(\frac{\partial^2 C}{\partial x_3^2}\right) + \frac{d_t}{d_\infty}\left(\frac{\partial T}{\partial x_3}\right)^2, \tag{5}$$

$$u_1 = U_{x_3},\ u_2 = V_{x_3},\ C = C_\infty,\ x_3 = 0 - c_f(T_f - T_{x_3}) = t_f\frac{\partial T}{\partial x_3},\quad \text{at}\quad x_3 = 0, \tag{6}$$

$$u_1 \to 0\ ,\ C \to \infty\ ,\ T \to \infty\ ,\ \text{at}\ x_3 \to \infty. \tag{7}$$

Eqs. (9)–(12) are the governing equations, and they involve several parameters that ν, T, C, and α represent viscosity, temperature, volumetric nanoparticle ratio, and thermal diffusivity, respectively. The Brownian, thermophoretic coefficients, and the balance of the heat capacity of carrier fluid and nanoparticles are represented by, d_b , d_t, and τ, respectively. To reduce the model equations to a dimensionless form, we use the following transformations:

$$u_1 = U_0 e^{\left(\frac{x_1+x_2}{L}\right)}F'\ ,\ u_2 = V_0 e^{\left(\frac{x_1+x_2}{L}\right)}G'\ ,\ u_3 = \left(\frac{\nu U_0}{2L}\right)^{\frac{1}{2}} e^{\left(\frac{x_1+x_2}{L}\right)}(F + \zeta F' + G + \zeta G'),$$

$$\theta = \frac{T - T_\infty}{T_f - T_\infty},\ \phi = \frac{C - C_\infty}{C_f - C_\infty}\ ,\ \zeta = \left(\frac{U_0}{2\nu L}\right)^{\frac{1}{2}} x_3 e^{\left(\frac{x_1+x_2}{2L}\right)}. \tag{8}$$

We obtain the following equations by plugging in these coordinates into Eq. (2)–(7), with Eq. (1) being satisfied uniquely:

$$F''' - 2(F'^2 + GF') + FF'' + GF'' - MF'' = 0, \tag{9}$$

$$G''' - 2(G'^2 + G'F') + FG'' + GG'' - MG'' = 0, \tag{10}$$

$$\frac{\theta''}{\Pr} - A(\theta G' + \theta F') + F\theta' + G\theta' + N_b\theta'\phi' + N_t\theta'^2 = 0, \tag{11}$$

$$\phi'' - A(\theta G' + \theta F') + F\theta' + G\theta' + N_b\theta'\phi' + N_t\theta'^2 = 0, \tag{12}$$

$$F(0) = 0,\ G(0) = 0,\ F'(0) = 1,\ G'(0) = \alpha, \text{and}\ \theta'(0) = -\text{Bi}(1 - \theta(0)),$$

$$\phi(0) = 1,\ F'(\infty) = 0,\ G'(\infty) = 0,\ \theta(\infty) = 0,\ \phi(\infty) = 0. \tag{13}$$

Eqs. (9)–(12) are the governing equations, and they involve several dimensionless parameters defined as: $M = \frac{\sigma B_0^2}{\rho L}$, $N_b = \tau d_b(C_{x_3} - C_\infty)/\nu$, $N_t = \tau d_t(T_{x_3} - T_\infty)/\nu$ represent the magnetic, Brownian, and thermophoretic parameters, respectively. The local Prandtl number, Biot number, and Schmidt number are represented by:

$\Pr = \frac{\nu}{\alpha}$, $\text{Bi} = \frac{c_f}{t_f}\left(\frac{2\nu L}{U_\circ}\right)^{\frac{1}{2}} e^{\frac{x_1+x_2}{2L}}$, $\text{Sc} = \frac{\nu}{d_b}$, respectively.

3 Methodology

The definition of the ith Haar wavelet family is as follows for $\zeta \in [A, B]$, where $A, B \in R$.

$$\psi_i(\zeta) = \begin{cases} 1\ , \text{ where } \zeta \in\ [t_1, t_2) \\ -1\ , \text{ where } \zeta \in\ [t_2, t_3) \\ 0\ , \text{elsewhere,} \end{cases} \tag{14}$$

with

$$t_1 = k/\bar{m}_1,\ t_2 = (k + 1)/2/\bar{m}_1, \text{ and } t_3 = k + 1/\bar{m}_1. \tag{15}$$

When it comes to wavelet analysis, each $2\bar{M}$ subinterval in the given domain $[A, B]$ has a uniform length of $\zeta = (B, A)/2\bar{M}$. The maximum resolution, $\bar{m}_1 = 2^j$, that may be achieved is represented by $\bar{M} = 2j$. The parameter $(\bar{M})$ indicates how many of these subintervals are examined in detail. The wavelet transformation is controlled by two complex parameters, the dilatation parameter, $j = 0, 1, \ldots J$. and $k = 0, 1, \ldots, \bar{m}_1 - 1$, the translation parameter. The formula for the wavelet number is represented as $i = \bar{m}_1 + k + 1$. Regarding the integrals of the Haar function,

$$p_{i1}(\zeta) = \int_0^\zeta \psi_i(\zeta), \tag{16}$$

$$p_{i,\,l+1}(x) = \int_0^\zeta p_{i,l}(\zeta)\mathrm{d}\zeta, \quad l = 1, 2,\ldots, \tag{17}$$

These integrals are computed using Eq. (14)

$$p_{i1}(\zeta) = \begin{cases} \zeta - t_1, & \text{for } \zeta \in [t_1, t_2) \\ t_3 - \zeta\ , & \text{for } \zeta \in [t_2, t_3) \\ 0, & \text{elsewhere,} \end{cases} \tag{18}$$

$$p_{i2}(\zeta) = \begin{cases} \frac{1}{2}(\zeta - t_1)^2\ , \text{ for } \zeta \in [t_1, t_2) \\ \frac{1}{4\bar{m}_1{}^2} - \frac{1}{2}(t_3 - \zeta)^2, \text{ for } \zeta \in [t_2, t_3) \\ \frac{1}{4\bar{m}_1{}^2}\ , \text{ for } \zeta \in\ [t_3, 1) \\ 0, \quad \text{elsewhere,} \end{cases} \tag{19}$$

$$p_{i3}(\zeta) = \begin{cases} \frac{1}{6}(\zeta - t_1)^3\ , \text{ for } \zeta \in [t_1, t_2) \\ \frac{1}{4\bar{m}_1{}^2}(\zeta - t_2) - \frac{1}{6}(t_3 - \zeta)^3, \text{ for } \zeta \in [t_2, t_3) \\ \frac{1}{4\bar{m}_1{}^2}(\zeta - 1, \text{ for } \zeta \in\ [t_3, 1) \\ 0, \quad \text{elsewhere.} \end{cases} \tag{20}$$

The notations are also presented as follows:

$$C_{i1} = \int_0^L p_{i1}(\zeta)\mathrm{d}\zeta, \tag{21}$$

$$C_{i2} = \int_0^L \psi_i(\zeta)\mathrm{d}\zeta. \tag{22}$$

The Haar wavelet function summation can be expressed as follows:

$$F(\zeta) = \sum_{i=1}^{\infty} a_i\psi_i(\zeta). \tag{23}$$

For the provided problems (9)–(12), we may approximate the highest-order derivatives of F, G, θ, and ϕ by using wavelets, which makes it easier to build a direct and precise approach of HWCM.

$$F'''(\zeta) = \sum_{i=1}^{2M} a_i\psi_i(\zeta), \tag{24}$$

$$G'''(\zeta) = \sum_{i=1}^{2M} b_i\psi_i(\zeta), \tag{25}$$

$$\theta''(\zeta) = \sum_{i=1}^{2M} c_i\psi_i(\zeta), \tag{26}$$

$$\phi''(\zeta) = \sum_{i=1}^{2M} d_i\psi_i(\zeta). \tag{27}$$

Eq. (24) is integrated to yield the corresponding values of $F'''(\zeta)$, $F''(\zeta)$, $F'(\zeta)$, and $F(\zeta)$.

$$F'''(\zeta) = \sum_{i=1}^{2M} a_i\left(p_{i,1}(\zeta) - \frac{1}{L}C_{i,1}\right), \tag{28}$$

$$F''(\zeta) = \sum_{i=1}^{2M} a_i\left(p_{i,2}(\zeta) - \frac{1}{L}\zeta C_{i,1}\right), \tag{29}$$

$$F'(\zeta) = \sum_{i=1}^{2M} a_i\left(p_{i,3}(\zeta) - \frac{1}{L}\frac{\zeta^2}{2}C_{i,1}\right), \tag{30}$$

$$F(\zeta) = \sum_{i=1}^{2M} a_i\left(p_{i,4}(\zeta) - \frac{1}{L}\frac{\zeta^3}{3}C_{i,1}\right). \tag{31}$$

Let (L) stand for a large number. Eqs. (24)–(31) can be substituted into Eqs. (9)–(12) to obtain a numerical solution for the ordinary differential equations. The following part presents a graphical depiction of the results obtained from the suggested solution.

4 Results and discussion

The influence of the magnetic field strength on $F'(\zeta)$ and $G'(\zeta)$ is seen in Figure 3. Results from this graphic illustrate that, for a given increasing parameter (M), there is a noticeable decrease in the boundary-layer thickness and

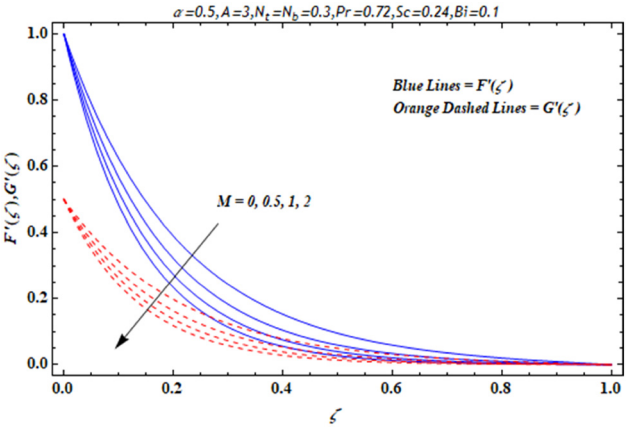

Figure 3: Evolutions of "M" on $F'(\zeta)$ and $G'(\zeta)$.

the velocity profile strength represented by the letters $F'(\zeta)$ and $G'(\zeta)$. This phenomenon has a physical basis, although a conductive fluid reacts to a magnetic field by having the ability to flow electricity, and the magnetic force acting within the boundary layer prevents the fluid from moving and causes it to slow down. In conclusion, the magnetic field regulates the gap between the boundary layers.

The impact of the ratio parameter on $F'(\zeta)$ and $G'(\zeta)$ is observed in Figure 4. The current phenomenon is reduced to 2D flow when $\alpha = 0$, while the problem is turned down to axisymmetric flow when $\alpha = 1$. In addition, as seen in Figure 4, the velocity $F'(\zeta)$ falls, while it $G'(\zeta)$ increases as the ratio parameter rises.

Figures 5 and 6 show that increasing the stretching ratio rate decreases temperature $\theta(\zeta)$ and nanoparticle concentration profile $\phi(\zeta)$. Results show that magnetic field strength raises nanofluid temperature and concentration. Magnetic parameter increases dimensionless

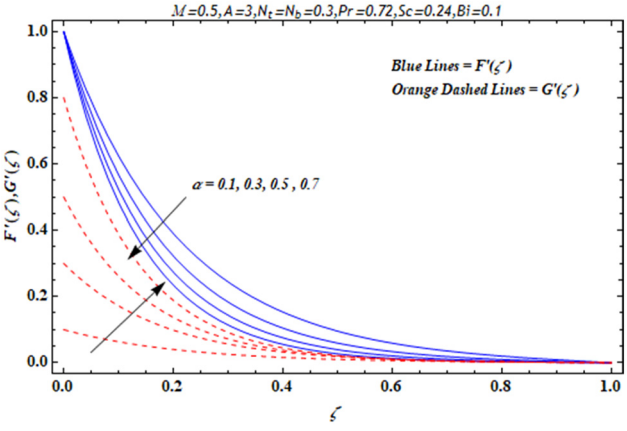

Figure 4: Evolutions of "α" on $F'(\zeta)$ and $G'(\zeta)$.

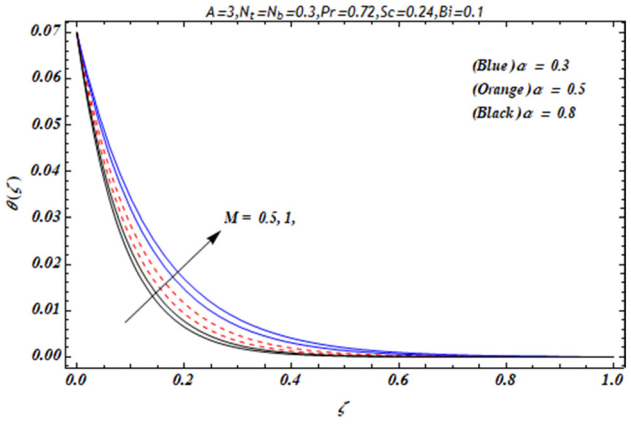

Figure 5: Evolutions of "M" and "α" on $\theta(\zeta)$.

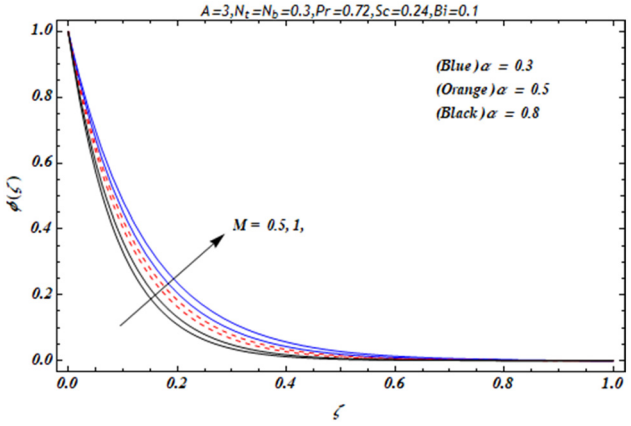

Figure 6: Evolutions of "M" and "α" on $\phi(\zeta)$.

temperature and nano-concentration profiles. Heat is produced because the Lorentz force resists fluid motion. More required magnetic fields thicken thermal and nanoparticle volume fraction boundary layers.

$\theta(\zeta)$ and $\phi(\zeta)$ over the sheet are graphically represented in Figures 7 and 8, respectively, showing the effects of changing the thermophoretic parameters (N_t) and Brownian motion parameter Nb values. A fascinating physical finding is revealed: an increase in the thermophoretic parameter (N_t) causes the thickness of the boundary layer to increase for both dimensionless functions. This finding clarifies the relationship between these parameters and the complex dynamics controlling the system. The thermophoretic force of a temperature gradient causes the flow to be accelerated away from the stretching surface. By doing so, heat is transferred from the surface, and (N_t) is raised. Figure 8 shows the thermophoretic influence of (N_t) on nanoparticle volume fraction $\phi(\zeta)$. As Nb grows, the nanoparticle volume fraction or concentration profile $\phi(\zeta)$ decreases.

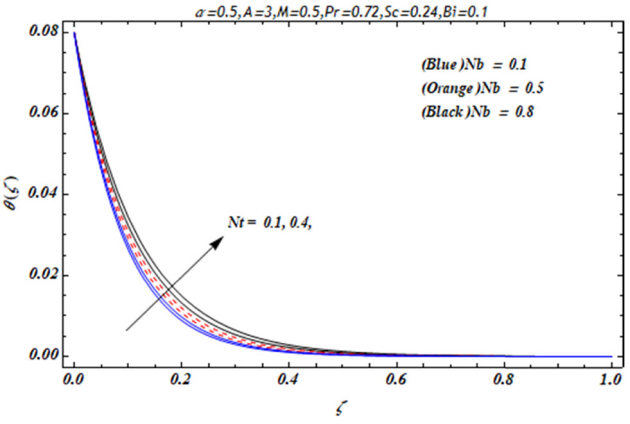

Figure 7: Evolutions of "Nt" and "Nb" on $\theta(\zeta)$.

Temperature and nano-concentration distributions as a function of the local Biot number (Bi) for varying temperature exponent parameter (A) values are depicted in Figures 9 and 10, respectively. It is shown that as (A) rises, so do the temperature and concentration profiles. The condition $A = -1$ cannot be the adiabatic case due to two more events in the energy equation. It has been noted that as the Biot number rises, so do the temperature and concentration profiles. The Biot number physically refers to the ratio of surface convection to internal conduction. Moreover, as the Biot number grows, so does the convection at the surface, causing an increase in surface temperature.

The impact of (Pr) and (Sc) on $\theta(\zeta)$ the temperature profile is depicted in Figure 11. The thermal concentration is more important than the concentration for fluids with low Prandtl numbers, like electrolyte solutions. We find that a decrease in thermal diffusivity is correlated with an increase in the Prandtl number (Pr), which in turn causes the thermal boundary layer to thin simultaneously. This decrease is consistent with a higher heat transfer rate

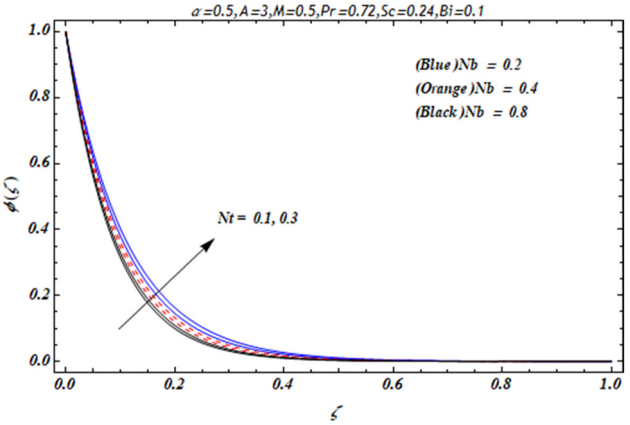

Figure 8: Evolutions of "Nt" and "Nb" on $\phi(\zeta)$.

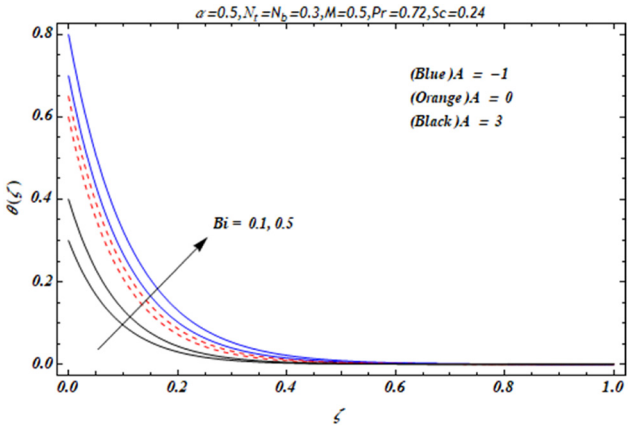

Figure 9: Evolutions of "Bi" and "A" on $\theta(\zeta)$.

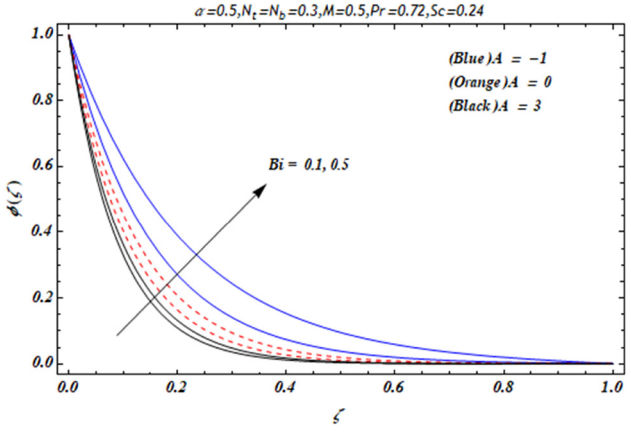

Figure 10: Evolutions of "Bi" and "A" on $\phi(\zeta)$.

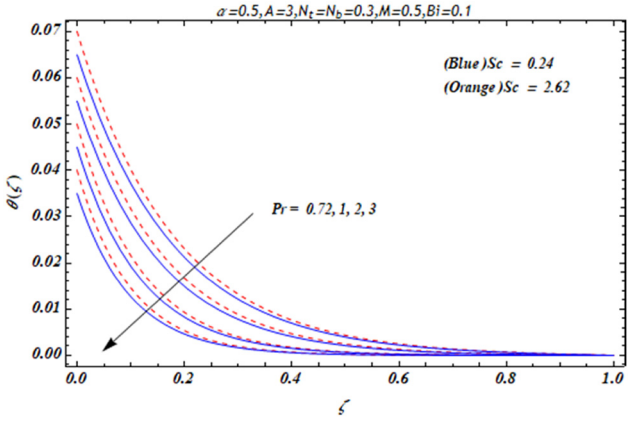

Figure 11: Evolutions of "Pr" and "Sc" on $\theta(\zeta)$.

at the sheet interface. Furthermore, an interesting finding occurs at higher Schmidt numbers (Sc): the temperature distribution shows local aberrations, especially near the stretched sheet. These results provide light on the complex

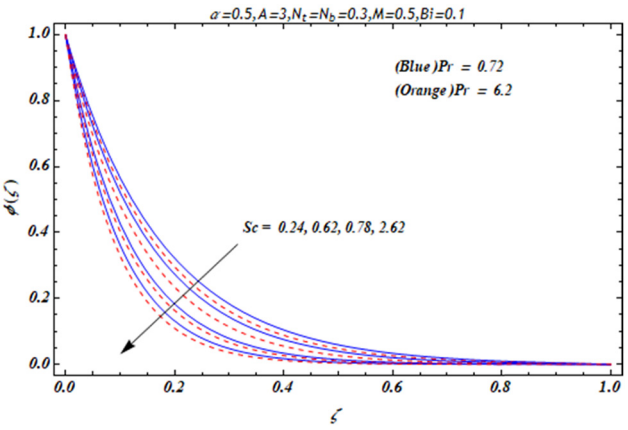

Figure 12: Evolutions of "Pr" and "Sc" on $\phi(\zeta)$.

thermal dynamics close to the boundary layer by highlighting the delicate interplay between Prandtl and Schmidt numbers.

Figure 12 shows that larger values of (Sc) correspond to a thinner concentration boundary layer due to a smaller Brownian diffusion coefficient DB. When the Prandtl number is large enough, the profiles show that SGH occurs (even for positive values of (A) Just beyond the stretching surface, $\phi(\zeta)$, it slightly decreases, while Pr slightly increases.

Table 1 displays a comparative examination of the HWCM findings in respect to previously obtained results. There is a clear and significant agreement between the two sets of results, as seen by the commendable congruence in values across several metrics. Tables 2 and 3 display the $-G''(0)$ and $-F''(0)$ values obtained using the HWCM solutions, respectively. These values are presented for various combinations of (M) and (α). More precisely, when

Table 1: Wall temperature gradient comparison [34,36] represented by $\theta'(0).B_i = M = \alpha = 0, Nt = Nb = 0.00001$.

Pr	A	$\theta'(0)$		
		[29]	[31]	Present HWCM
	0	−0.54964375	−0.549641	−0.549643407
	1	−0.95478270	−0.954763	−0.9547826971
	3	−1.56029540	−1.560175	−1.5605674022
5	−1.5	1.35324050	1.353250	1.3532405205
	0	−1.52123900	−1.521662	−1.5212389982
	1	−2.50013157	−2.500653	−2.5001315727
	3	−3.88655510	−3.886678	−3.8866541019
10	−1.5	2.20002816	2.200456	2.2009643651
	0	−2.25742372	−2.259142	−2.25745437184
	1	−3.66037218	−3.662782	−3.6605671782
	3	−5.62819631	−5.630445	−5.62816053101

Table 2: Link between the parameters, Pr = 0.5, Sc = 0.2, B_i = 0.1, and A = 2.5, by showing numerical values of $G''(0)$ at the sheet's surface that correspond to different combinations of (M) and (α).

M	α	$G''(0)$	
		iteration	HWCM
0	0.5	89	0.784943489
0.5		34	0.8621073370
1.0		25	0.9324605413
1.5		21	0.9976634541
2.0		18	1.0587435990
0.5	0.6	31	1.0627548401
	0.7	29	1.2719543637
	0.8	26	1.4894654082
	0.9	28	1.7146934784

Table 3: Link between the parameters, Pr = 0.5, Sc = 0.2, Bi = 0.1, and A = 2.5, by showing numerical values of $F''(0)$ at the sheet's surface that correspond to different combinations of (M) and (α)

M	α	$F''(0)$	
		Iteration	HWCM
0	0.5	89	1.5698884578
0.5	0.6	34	1.7242436741
1.0	0.7	25	1.8643610826
1.5	0.8	21	1.9953271033
2.0	0.9	18	2.1176791980
0.5		31	1.7712565668
	0.6	29	1.8170650624
	0.7	26	1.8617663102
	0.8	28	1.9053449760

keeping (α) a constant value of 0.5, an increase in (M) results in an increase in both $-G''(0)$ and $-F''(0)$. Similarly, keeping (M) constant at a value of 0.5 shows that increasing the parameter results in the improvement of both $-G''(0)$ and $-F''(0)$.

5 Conclusion

The investigations that came before are prompted, in large part, by the features of the MHD flow of nanofluid over a stretching sheet under convective conditions. These characteristics have been investigated in great detail. Following the transformation of the governing equations into a system of coupled nonlinear differential equations, a novel method known as the HWCM was applied to find a solution to the equations. The proposed approach is highly adaptable in dealing with irregular domains and providing localized, multiresolution solutions. Nevertheless, one should take into account the susceptibility of the system to the Gibbs phenomenon, its restricted smoothness, and the potential difficulties arising from nonlinearities and slower convergence rates. When studying the MHD flow model over an exponentially stretched sheet with convective heating, it is important to pay attention to accurately capturing magnetic fields, fluid dynamics, and temperature distributions. Ensuring numerical stability, verifying against established solutions, and mitigating potential thermal instabilities are essential for achieving precise and dependable outcomes in this particular application.

When the temperature exponent (A) is decreased to specific negative values, the profile of the temperature increases. As a result, the parameters' effect on the temperature gradient along the wall is reversed when $A = -1$, relative to the case when $A \geq 0$. The temperature rises as the Brownian motion parameter (Nb) rises, but the concentration of nanoparticles falls.

Acknowledgments: Princess Nourah bint Abdulrahman University Researchers Supporting Project number (PNURSP2024R183), Princess Nourah bint Abdulrahman University, Riyadh, Saudi Arabia. This work was supported by the Deanship of Scientific Research, Vice Presidency for Graduate Studies and Scientific Research, King Faisal University, Saudi Arabia (Grant No. 5332).

Funding information: Princess Nourah bint Abdulrahman University Researchers Supporting Project number (PNURSP2024R183), Princess Nourah bint Abdulrahman University, Riyadh, Saudi Arabia. This work was supported by the Deanship of Scientific Research, Vice Presidency for Graduate Studies and Scientific Research, King Faisal University, Saudi Arabia [Grant No. 5332].

Author contributions: All authors have accepted responsibility for the entire content of this manuscript and approved its submission.

Conflict of interest: The authors state no conflict of interest.

References

[1] Sun L, Liang T, Zhang C, Chen J. The rheological performance of shear-thickening fluids based on carbon fiber and silica nanocomposite. Phys Fluids. 2023;35(3):32002. doi: 10.1063/5.0138294.

[2] Xiang G, Yang T, Guo J, Wang J, Liu B, Chen S. Optimization transient wear and contact performances of water-lubricated bearings under fluid-solid-thermal coupling condition using profile modification. Wear. 2022;502–503:204379. doi: 10.1016/j.wear.2022.204379.
[3] Kuang W, Wang H, Li X, Zhang J, Zhou Q, Zhao Y. Application of the thermodynamic extremal principle to diffusion-controlled phase transformations in Fe-C-X alloys: Modeling and applications. Acta Materialia. 2018;159:16–30. doi: 10.1016/j.actamat.2018.08.008.
[4] Zheng B, Lin D, Qi S, Hu Y, Jin Y, Chen Q, et al. Turbulent skin-friction drag reduction by annular dielectric barrier discharge plasma actuator. Phys Fluids. 2023;35(12):125129. doi: 10.1063/5.0172381.
[5] Hu G, Ying S, Qi H, Yu L, Li G. Design, analysis and optimization of a hybrid fluid flow magnetorheological damper based on multiphysics coupling model. Mech Syst Signal Process. 2023;205:110877. doi: 10.1016/j.ymssp.2023.110877.
[6] Pattanaik PC, Mishra SR, Jena S, Pattnaik PK. Impact of radiative and dissipative heat on the Williamson nanofluid flow within a parallel channel due to thermal buoyancy. Proc Inst Mech Eng Part N: J Nanomater Nanoeng Nanosyst. 2022 Mar;236(1–2):3–18.
[7] Phelan PE, Taylor R, Adrian RJ, Prasher RS, Otanicar TP. Light-induced energy conversion in liquid nanoparticle suspensions. Nanopart Heat Transf Fluid Flow. 2012 Dec 4;4:123–42.
[8] Trieb F, Nitsch J. Recommendations for the market introduction of solar thermal power stations. Renew Energy. 1998 May;14(1–4):17–22.
[9] Ladjevardi SM, Asnaghi A, Izadkhast PS, Kashani AH. Applicability of graphite nanofluids i-n direct solar energy absorption. Sol Energy. 2013 Aug;94:327–4.
[10] Jena S, Mishra SR, Pattnaik PK. Development in the heat transfer properties of nanofluid due to the interaction of inclined magnetic field and non-uniform heat source. J Nanofluids. 2020 Sep;9(3):143–51.
[11] Mushtaq A, Mustafa M, Hayat T, Alsaedi A. Nonlinear radiative heat transfer in the flow of nanofluid due to solar energy: A numerical study. J Taiwan Inst Chem Eng. 2014;45:1176.
[12] Munir A, Shahzad A, Khan M. Forced convective heat transfer in boundary layer flow of sisko fluid over a nonlinear stretching sheet. PLoS ONE. 2014;9:2100056.
[13] Uddin MJ, Beg OA, Khan WA, Ismail AI. Effect of Newtonian heating and thermal radiation on heat and mass transfer of nanofluids over a stretching sheet in porous media. Heat Transf Asian Res. 2014;44:681–95.
[14] Shen M, Wang F, Chen H. MHD mixed convection slip flow near a stagnation-point on a nonlinearly vertical stretching sheet. Bound Value Probl. 2015;2015:78.
[15] Upreti H, Bartwal P, Pandey AK, Makinde OD. Heat transfer assessment for Au-blood nanofluid flow in Darcy-Forchheimer porous medium using induced magnetic field and Cattaneo-Christov model. Numer Heat Transfer Part B: Fundam. 2023;84(4):415–31.
[16] Hsiao KL. Stagnation electrical MHD nanofluid mixed convection with slip boundary on a stretching sheet. Appl Therm Eng. 2016 Apr;98:850–61.
[17] Naramgari S, Sulochana C. Dual solutions of radiative MHD nanofluid flow over an exponentially stretching sheet with heat generation/absorption. Appl Nanosci. 2016 Jan;6:131–9.
[18] Pandey AK, Upreti H, Joshi N, Uddin Z. Effect of natural convection on 3D MHD flow of MoS_2–GO/H2O *via* porous surface due to multiple slip mechanisms. J Taibah Univ Sci. 2022;16(1):749–62.
[19] Hayat T, Ullah I, Alsaedi A, Farooq M. MHD flow of Powell-Eyring nanofluid over a non-linear stretching sheet with variable thickness. Results Phys. 2017 Jan;7:189–96.
[20] Ghosh S, Mukhopadhyay S. MHD mixed convection flow of a nanofluid past a stretching surface of variable thickness and vanishing nanoparticle flux. Pramana. 2020 Dec;94:1–2.
[21] Upreti H, Pandey AK. MHD tangent hyperbolic fluid flow over stretching sheet with Cattaneo-Christov heat flux model and quadratic convection: A statistical analysis. In Mathematical modeling of fluid dynamics and nanofluids. Boca Raton: CRC Press; 2023. p. 84–100.
[22] Makinde OD, Mishra SR. Chemically reacting MHD mixed convection variable viscosity Blasius flow embedded in a porous medium. In Defect and diffusion forum 2017 May 31. Vol. 374; Switzerland: Trans Tech Publications Ltd. p. 83–91.
[23] Nisar KS, Mohapatra R, Mishra SR, Reddy MG. Semi-analytical solution of MHD free convective Jeffrey fluid flow in the presence of heat source and chemical reaction. Ain Shams Eng J. 2021 Mar;12(1):837–45.
[24] Mishra SR, Hoque MM, Mohanty B, Anika NN. Heat transfer effect on MHD flow of a micropolar fluid through porous medium with uniform heat source and radiation. Nonlinear Eng. 2019 Jan;8(1):65–73.
[25] Shah NA, Wakif A, Shah R, Yook SJ, Salah B, Mahsud Y, et al. Effects of fractional derivative and heat source/sink on MHD free convection flow of nanofluids in a vertical cylinder: A generalized Fourier's law model. Case Stud Therm Eng. 2021;28:101518.
[26] Zhang XH, Shah R, Saleem S, Shah NA, Khan ZA, Chung JD. Natural convection flow Maxwell fluids with generalized thermal transport and Newtonian heating. Case Stud Therm Eng. 2021;27:101226.
[27] Nadeem S, Khan AU, Saleem S. A comparative analysis on different nanofluid models for the oscillatory stagnation point flow. Eur Phys J Plus. 2016 Aug;131:1–4.
[28] Nawaz M, Nazir U, Saleem S, Alharbi SO. An enhancement of thermal performance of ethylene glycol by nano and hybrid nanoparticles. Phys A: Stat Mech Appl. 2020 Aug;551:124527.
[29] Saleem S, Al-Qarni MM, Nadeem S, Sandeep N. Convective heat and mass transfer in magneto Jeffrey fluid flow on a rotating cone with heat source and chemical reaction. Commun Theor Phys. 2018 Nov;70(5):534.
[30] Rashidi MM, Kavyani N, Abelman S, Uddin MJ, Freidoonimehr N. Double diffusive magnetohydrodynamic (MHD) mixed convective slip flow along a radiating moving vertical flat plate with convective boundary condition. PLoS One. 2014 Oct;9(10):e109404.
[31] Lepik U. Haar wavelet method for nonlinear integrodifferential equations. Appl Math Comput. 2006;176:324–33.
[32] Lepik U. Numerical solution of evolution equations by the Haar wavelet method. Appl Math Comput. 2007;185:695–704.
[33] Šarler B, Aziz I. Haar wavelet collocation method for the numerical solution of boundary layer fluid flow problems. Therm Sci. 2011;50:686–97.
[34] Liu IC, Wang HH, Peng YF. Flow and heat transfer for three-dimensional flow over an exponentially stretching surface. Chem Eng Commun. 2013 Jan;200(2):253–68.
[35] Nield DA, Kuznetsov AV. The Cheng–Minkowycz problem for natural convection about a vertical plate embedded in a tridisperse porous medium. Int J Heat Mass Transf. 2011 Jul;54(15–16):3485–93.
[36] Khan WA, Pop I. Boundary-layer flow of a nanofluid past a stretching sheet. Int J Heat Mass Transf. 2010 May;53(11–12):2477–83.